Macromolecules
ARTICLE

Macromolecules **2009**, *42*, 7299–7308 **7299**
DOI: 10.1021/ma9002193

New Poly(methyl methacrylate)/*n*-Butyl Acrylate/Pentafluorostyrene/ Poly(ethylene glycol) (p-MMA/nBA/PFS/PEG) Colloidal Dispersions: Synthesis, Film Formation, and Protein Adsorption

Anuradha Misra, William L. Jarrett, and Marek W. Urban*

School of Polymers and High Performance Materials, Shelby F. Thames Polymer Science Research Center, The University of Southern Mississippi, Hattiesburg, Mississippi 39406

Received February 3, 2009; Revised Manuscript Received August 24, 2009

ABSTRACT: A new family of water-dispersible colloidal particles composed of poly(methyl methacrylate/*n*-butyl acrylate/pentafluorostyrene/poly(ethylene glycol) dimethacrylate) (p-MMA/nBA/PFS/PEG) copolymers which coalesce at room temperature was developed using free radical emulsion polymerization. These stable colloidal dispersions contain up to 30% w/w PEG and 35% w/w PFS and exhibit core−shell morphologies that consist of the p-MMA/nBA/PFS core and the PEG shell. Incorporation of PFS not only enhances the inhibition of the protein adsorption but also results in mechanically stable solid polymeric films. Solid-state 2D NMR, internal reflection infrared imaging (IRIRI), and atomic force microscopy (AFM) analysis showed that after coalescence the surface contains PEG-rich components which, combined with fluorinated domains, result in hydrophobic and hydrophilic segments that inhibit protein adsorption. Adsorption of bovine serum albumin (BSA), lipopolysacharide (Lipopoly), and fibrinogen (Fib) on p-MMA/nBA/PFS and p-MMA/nBA/PFS/PEG (5, 10, 20, and 30%) film surfaces revealed that the proteins exhibit higher affinity toward p-MMA/nBA/PFS surfaces, whereas PEG incorporated into p-MMA/nBA/PFS colloidal particles counter this behavior, and the compositional balance between PFS and PEG heterogeneities minimizes the protein adsorption. Incorporation of PFS is essential because when copolymerized, not only helps inhibiting protein adsorption but also facilitates mechanical integrity of the films.

Introduction

Controllable adsorption-to or desorption-from polymeric surfaces of biologically active species have been ofconsiderable interest, and numerous studies advanced understanding of interactions governing forces responsible for these processes.[1−3] One quantity that relates the adhesion strength (A) of a fouling organism to the surface energy (γ) and modulus (E) of the surface is expressed as $A = \sqrt{\gamma E}$.[3] Among many promising polymeric materials with low surface energies, fluoropolymers (FPs) exhibit relatively low friction,[4−7] but their high modulus often overrides other useful properties. On the other hand, thermoplastic elastomers, such as styrene−ethylene/butylene−styrene (SEBS) block copolymers, offer desirable mechanical properties, but elevated surface energies result in a high adhesion strength to protein molecules.[8] In contrast, poly(ethylene glycol) (PEG) exhibits low protein adsorption values, low toxicity, and acceptable compatibility with biological systems, and its incorporation into other polymeric coatings has been shown to inhibit protein adsorption, thereby reducing the adhesion strength of bioorganisms.[9,10] The presence of the PEG layer shields the surface by introducing the high activation barrier for proteins to adsorb to surfaces, and the chain length as well as the surface coverage was shown to impart protein resistance.[11−16] Another useful feature of PEG was shown upon its incorporation into polyurethanes which resulted in a distinct phase separation.[17−19] Taking advantage of the PEG properties as well as the low surface energy of FPs, other successful approaches focused on achieving desired physicochemical properties by controlled synthesis of fluorinated and PEGylated networks using atom transfer radical polymerization.[1,2,20−22] Other approaches included patterning of surfaces with fluorinated and PEG phases,[23] formation of cross-linked networks,[8,24] and surface grafting of PEG and fluoropolymers to surfaces.[25−27] Although it is well established that the presence of PEG provides environments conducive for protein desorption, the presence of other components also plays a significant synergistic role. For this reason and to increase mechanical integrity of otherwise fragile polymer networks we incorporated PFS.

In the view of these considerations, the syntheses of environmentally benign colloidal particles containing PEG and FPs that upon coalescence form polymeric films have not been exploited. If successful, this approach will offer a new platform of aqueous colloids that exhibit antifouling characteristics. Particular challenges are to combine low surface tension fluoromonomers which impose severe restrictions on polymerization in aqueous environments with methacrylates and acrylates. The first part of this study describes the synthesis of pentafluorostyrene (PFS), methyl methacrylates (MMA), *n*-butyl acrylate (nBA), and PEG that form colloidal particles, whereas the second will discuss stratification processes during coalescence of p-MMA/nBA/PFS/PEG particles which result in stratified films that inhibit protein adsorption.

Experimental Section

MMA, nBA, PFS, PEG (mol wt = 750), and sodium dioctylsulfosuccinate (SDOSS) were purchased from Aldrich Chemical Co. Water-soluble initiator 2,2′-azobis[2-(2-imidazolin-2-yl)propane] dihydrochloride (VA-44) was purchased from Wako Pure Chemicals Ind. Ltd. Purity of all components was greater than 99.9%.

p-MMA/nBA/PFS/PEG emulsions were synthesized using a semicontinuous process outlined elsewhere[28,29] and adapted for small-scale polymerization. The reaction flask was placed in a water bath set at 50 °C, purged with N_2 gas, and charged with

*To whom all correspondence should be addressed. E-mail: marek.urban@usm.edu.

Published on Web 09/10/2009

Table 1. Particle Size and Composition of p-MMA/nBA/PFS/PEG Colloidal Dispersions Synthesized with Different Copolymer Compositions

composition	p-MMA/ nBA/PFS	p-MMA/nBA/ PFS/PEG (5%)	p-MMA/nBA/ PFS/PEG (10%)	p-MMA/nBA/ PFS/PEG (20%)	p-MMA/nBA/ PFS/PEG (30
individual components (w/w %)	(A)	(B)	(C)	(D)	(E)
DDI	79	79	79	79	79
methyl methacrylate	2.1	2.1	2.1	2.1	2.1
n-butyl acrylate	11.6	10.5	9.5	7.4	5.3
PFS	7.4	7.4	7.4	7.4	7.4
PEG	0	1.05	2.1	4.2	6.3
SDOSS	0.63	0.63	0.63	0.63	0.63
VA-044	0.04	0.04	0.04	0.04	0.04
solids (%)	21	21	21	21	21
particle size (nm)	62	66	70	85	106

35 mL of DDI water under continuous stirring at 300 rpm. SDOSS surfactant was utilized, and Table 1 provides compositional ratios of colloidal dispersions prepared for the purpose of these studies. SDOSS was dissolved in water under high agitation followed by addition of monomers to produce a semistable pre-emulsion. The pre-emulsion was fed continuously over a period of 4 h while the initiator solution was added for 4.5 h. Upon completion of the initiator feed, polymerization was allowed to continue for another 10 h. This process resulted in 21% w/w solids which was determined from the initial feed composition of the initiator monomer mixture and the analysis of the solid content after the synthesis. As listed in Table 1, the following compositions of colloidal particles containing (A) p-MMA/nBA/PFS, (B) p-MMA/nBA/PFS/PEG (5% w/w), (C) p-MMA/nBA/PFS/PEG (10% w/w), (D) p-MMA/nBA/PFS/PEG (20% w/w), and (E) p-MMA/nBA/PFS/PEG (30% w/w) were prepared, and their particle size was analyzed using a Microtrac UPA 250 instrument. Molecular weight was determined using gel permeation chromatography (GPC) system which consisted of a Waters Alliance 2695 separation module, a Waters 2410 interferometric refractometer, and two polymer hexafluoroisopropanol (PL HFIP) gel columns (Polymer Laboratories Inc.; currently Varian) connected in series. Freshly distilled hexafluoroisopropanol (HFIP) serves as the mobile phase with a flow rate of 1.0 mL/min. Sample concentrations were 10−12 mg/mL in freshly distilled HFIP, with an injection volume of 50 μL. The detector signals were recorded using Empower 2 Chromatography Data Software (Waters Corp.), and molecular weights were determined relative to narrow molecular weight p-MMA standards. The number-average molecular weight of p-MMA/nBA/PFS copolymer was observed to be 1.5×10^5 g/mol. Because of cross-linking after PEG incorporation, the molecular weight for the p-MMA/nBA/PFS/PEG copolymer samples could not be obtained due to their insolubility in HFIP solvent.

Colloidal particle solutions were allowed to coalesce for 72 h at 23 °C and 70% relative humidity (RH) to form ~10 μm thick films. The films were obtained by a draw down on the poly(vinyl chloride) (PVC) substrates. For contact angle measurements as well as atomic force microscopy (AFM) experiments colloidal solutions were coalesced on a glass slides using a draw bar to give a film thickness of ~10 μm.

Solid-state ^{13}C NMR spectroscopy was performed on solid films using a Varian ^{UNITY}INOVA spectrometer equipped with a standard Chemagnetics 7.5 mm PENCIL-style probe and operating at a frequency of 100.6 MHz for carbon in order to determine copolymer composition. Films were loaded into zirconia rotor sleeves, sealed with Teflon caps, and spun at rate of 4.0 kHz. The standard cross-polarization/magic angle spinning (CP/MAS) technique was used with high-power proton decoupling implemented during data acquisition. The acquisition parameters were as follows: The ^{1}H 90° pulse width was set at 5.25 μs, the cross-polarization contact time was 1 ms, the dead time delay was 6.4 μs, and the acquisition time was 45 ms.[30] A recycle delay of 3 s between scans was utilized.

In order to analyze copolymer morphologies, solid-state wide-line separation (WISE) NMR spectroscopy was performed. The following parameters were utilized: a ^{1}H 90° pulse width of 5.25 μs, a cross-polarization contact time of 250 μs, a dead time delay of 5.9 μs, and an acquisition time of 45 ms. A recycle delay of 3 s between scans was utilized. Proton line shapes via F1 projections were taken using mixing times of 0 and 7.5 ms.[31,32] For WISE spectra, the spectral widths in ^{1}H and ^{13}C were 1250 and 301 ppm, respectively. The number of free induction decays (FID) acquired was 128, with 128 scans per FID. Time-proportional phase incrimination (TPPI) phase cycling was used to obtain phase-sensitive data, with an additional 384 points added to the indirectly detected dimension via linear prediction. Both dimensions were zero-filled to 2048 points, with Lorentzian and Gaussian apodization applied prior to Fourier transformation.

Microscopic attenuated total reflectance Fourier transform infrared (ATR FT-IR) spectroscopy measurements were conducted on the film−air (F−A) interfaces using a Bio-Rad FTS-6000 FT-IR single-beam spectrometer at a 4 cm^{-1} resolution. The surfaces were analyzed using a 2 mm Ge crystal with a 45° angle maintaining constant contact pressure between the crystal and the specimens. All spectra were corrected for spectral distortions using the Urban−Huang algorithm.[33] Internal reflection infrared imaging (IRIRI) experiments were conducted on a Varian Stingray system. This system consists of a Bio-Rad FTS 6000 spectrometer, a UMA 500 microscope, an Image IR focal plane array (FPA) image detector, and a semispherical germanium IRE. IRIR images were collected using the following spectral acquisition parameters: under sampling ratio 2, step-scan speed 5 Hz, and spectral resolution 8 cm^{-1} and the use of a Ge crystal in contact with the analyzed surface allows spatial resolution in the range of 1 μm.[34] In a typical experiment, spectral data set acquisition time was 2 min, and image processing was performed using ENVI software (The Environment for Visualizing Images, Research Systems, Inc.) version 3.5. When appropriate, baseline correction algorithms were applied to compensate for baseline deviations which were accomplished by built-in application software supplied by GRAMS/A1 v 7.02 (Galactic Ind.).

Atomic force microscopy (AFM) measurements were conducted on a Nanoscope IIIa Dimension 3000 scanning probe microscope (Digital Instruments). A silicon probe with 125 μm long silicon cantilever, nominal force constant of 40 N/m, and resonance frequency of 275 kHz were used in a tapping mode, allowing estimation of surface topography and roughness. Surface tension measurements were obtained using a FTA200 dynamic contact angle analyzer.[35] Zeta potential measurements were conducted on a Malvern Zetasizer nano-ZS using diluted colloidal dispersion in DI water at room temperature.

Bovine serum albumin (BSA), lipopolysacharide (Lipopoly), and fibrinogen (Fib) proteins were purchased from Aldrich Chemical Co. and were dissolved in phosphate buffer saline (PBS) solution (pH 7.0) at a concentration level of 8 mg/mL. Films containing copolymers p-MMA/nBA/PFS, p-MMA/nBA/PFS/PEG (5% w/w), p-MMA/nBA/PFS/PEG (10% w/w),

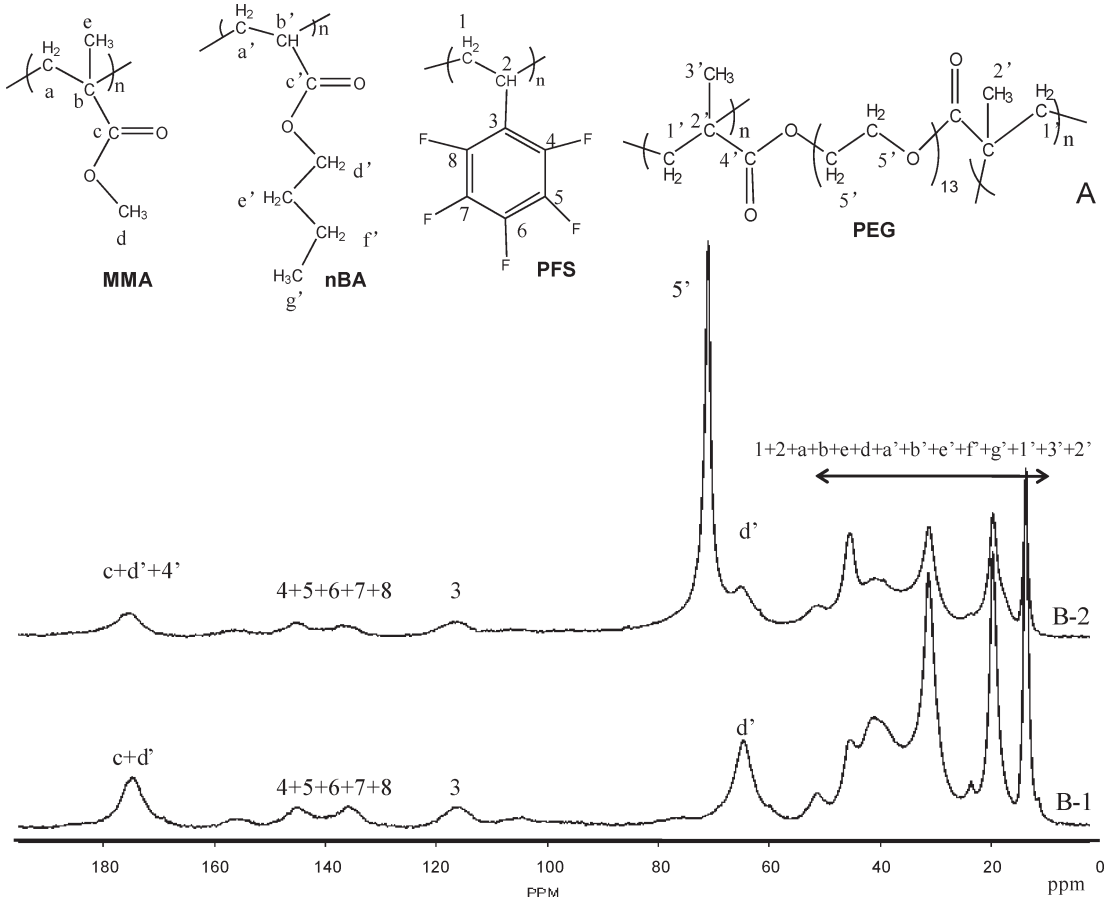

Figure 1. (A) Monomer structures. (B) Solid-state ^{13}C NMR spectra of p-MMA/nBA/PFS (B-1) and p-MMA/nBA/PFS/PEG (30%) (B-2) colloidal films.

p-MMA/nBA/PFS/PEG (20% w/w), and p-MMA/nBA/PFS/PEG (30% w/w) were equilibrated in the respective protein solutions by depositing 2 mL of solution on the films for 2 h at ambient temperature, followed by continuous rinsing the surface for 10 min with PBS solution to remove excess protein, followed by drying in a desiccator. Protein adsorptions on polymeric surfaces after drying were evaluated using ATR FT-IR spectroscopy and IRIRI.

Results and Discussion

As stated in the Introduction, the objective of these studies is to develop a new family of colloidal dispersions containing PFS and PEG components copolymerized with MMA and nBA monomers that upon coalescence form films that will repel proteins. The first part of this study will describe synthetic steps involved in the preparation of colloidal dispersions and their solution morphologies, whereas the remaining parts will focus on the particle coalescence and protein adsorption.

Synthesis of p-MMA/nBA/PFS/PEG Colloidal Dispersions. For the purpose of these studies we synthesized p-MMA/nBA/PFS copolymer particles containing 0, 5, 10, 20, and 30% w/w of PEG. Table 1 provides detailed compositions of the dispersions, % solids, and the particle size analysis data. To optimize the glass transition temperature (T_g) of the final compositions, the amount of nBA was varied from 25 to 55% w/w balanced by the equivalent amount of PEG to maintain the same % w/w solids. Their compositions are given in Table 1.

To determine whether all monomers were copolymerized to form p-MMA/nBA/PFS/PEG copolymer colloidal particles, solid-state ^{13}C NMR spectroscopy was utilized. Figure 1A shows chemical structures of MMA, nBA, PFS, and PEG, while solid-state ^{13}C NMR spectra of p-MMA/nBA/PFS and p-MMA/nBA/PFS/PEG (30%) are illustrated in B-1 and B-2 of Figure 1, respectively. The spectrum labeled B-1 clearly shows the resonances due to MMA, nBA, and PFS copolymer structures, and the solid-state ^{13}C NMR spectrum of p-MMA/nBA/PFS/PEG (30%) is illustrated in Figure 1B-2 and exhibits a large 70.1 ppm resonance due to $O-CH_2$ groups, indicating that PEG is copolymerized with MMA, nBA, and PFS monomers.

In an effort to determine the copolymer compositions of the colloidal particles, 2D NMR WISE experiments were conducted to monitor the chain dynamics by measuring the ^1H line width as a function of mixing time. The premise behind these experiments is that if copolymerized monomers units are randomly distributed, the 1H line width will approach a uniform value with increasing mixing time. In contrast, for block copolymers, the line will differ. In view of these considerations and structural features of p-MMA/nBA/PFS/PEG, the following carbon sites illustrated in Figure 2a, traces A−D, for 0 ms mixing time are of particular interest: 14.0 ppm due to the CH_3 resonance of nBA (A), 31.4 ppm due to the CH_2- resonance of MMA and nBA (B), 45.1 ppm due to the CH− resonance of PFS (C), and 70.7 ppm resonance due to the $-O-CH_2-$ of the PEG component (D). As shown, each of these resonances exhibits their own intrinsic ^1H line-width characteristic of their environment. Figure 2b illustrates the same experiment, but the mixing time was increased to 7.5 ms. As shown, the line width is the same for the resonances due to of nBA (trace A′), MMA and nBA (trace B′), and PFS (trace C′). At the same, the

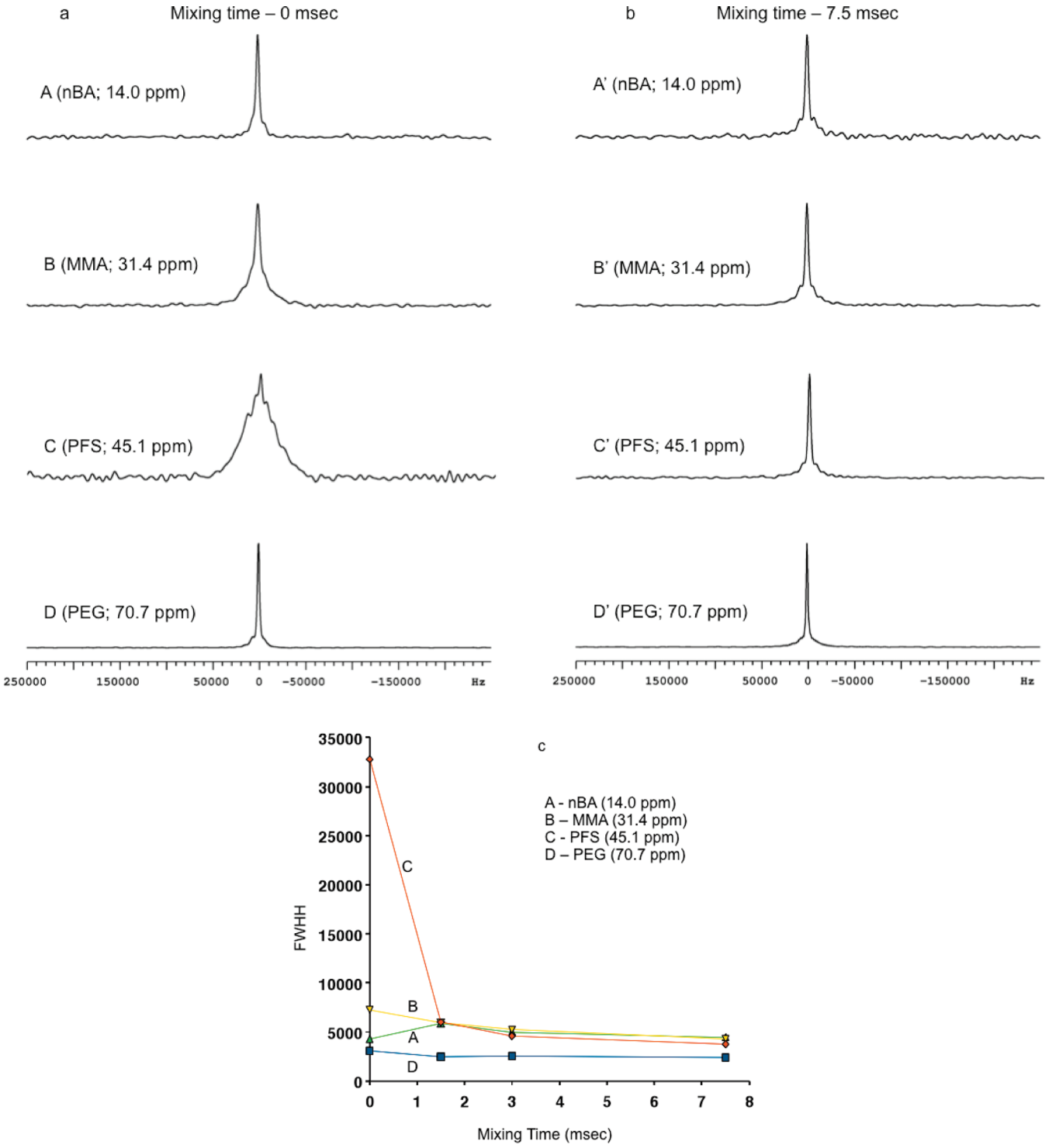

Figure 2. Stack plots of ^{1}H F1 traces from ^{13}C WISE 2D NMR data for p-MMA/nBA/PFS/PEG (30%) copolymer at 0 ms (a) and 7.5 ms (b) contact times. Traces A/A′: 14.0 ppm due to $-CH_3$ resonance of nBA; traces B/B′: 31.4 ppm due to due to $-CH_2-$ resonance of MMA and nBA; traces C/C′: 45.1 ppm due to $-CH-$ resonance of PFS; traces D/D′: 70.7 ppm due to $-O-CH_2-$ resonance of PEG. (c) is a plot of ^{1}H fwhh line width of selected sites as a function of mixing time. The error in measured line width (±400 Hz) is approximately the size of the data symbols.

resonance due to PEG remains unchanged. These results confirm close proximity of MMA, nBA, and PFS monomers due to their random copolymerization. However, the ^{1}H full width at half-height (fwhh) for the PEG moiety at 70.7 ppm remains unchanged and is significantly lower, which is consistent with earlier assessments that PEG is being copolymerized, but remaisn as a phase-separated entity with the copolymer. As will be seen later, these results are in agreement with the AFM and IRIRI analysis. In an effort to graphically illustrate the ^{1}H fwhh of these resonances, Figure 2c also illustrates the fwhh plotted as a function of mixing time. The corresponding ^{1}H fwhh for the 14.0, 31.4, and 45.1 ppm resonances decrease with the mixing time, whereas the 70.7 ppm ^{1}H fwhh remains unchanged. Figure 2c also illustrates that the ^{1}H fwhh of selected sites for the MMA, nBA, and PFS monomers converge to a similar value due to ^{1}H spin diffusion that is significantly broader than that of the PEG component.

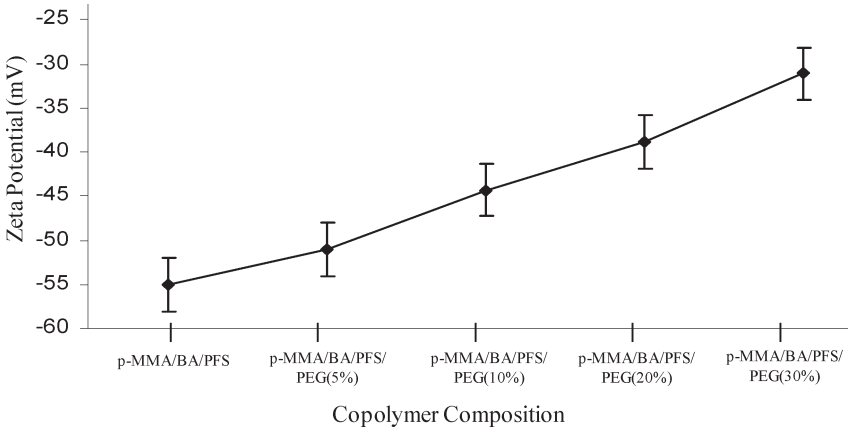

Figure 3. Zeta potential plotted as a function of copolymer composition of p-MMA/nBA/PFS/PEG colloidal dispersions.

Scheme 1. Schematic Representation of (A) Block Copolymerization of PEG Phase during Emulsion Polymerization Process and (B) Coalescence Mechanism for p-MMA/nBA/PFS/PEG Colloidal Dispersions Containing SDOSS Association with PEG Phase

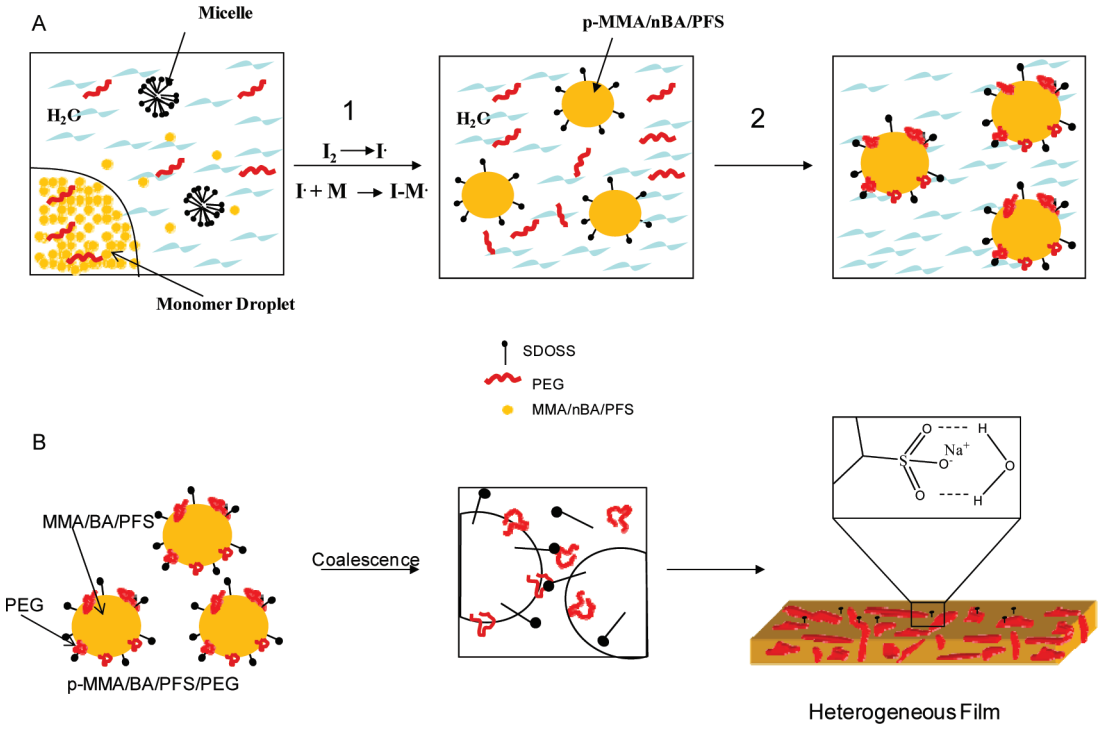

Table 1 also shows that the particle size of colloidal particles increases from 62 to 106 nm as the amount of PEG incorporated into p-MMA/nBA/PFS increases from 0 to 30% w/w, while a 20% w/w solids is retained. Although it is unlikely that the increase of the particle size with the increase PEG content is attributed to free volume increase since the T_g of both p-nBA and p-PEG are −54 and −42 °C, respectively,[36] zeta potential measurements were conducted on the diluted solutions at room temperature. As illustrated in Figure 3, as the amount of PEG increases from 0 to 30% w/w, zeta potential changes from −55 to −32 mV. The linear increase of the zeta potential is attributed to the displacement of surfactant molecules from the surface of the particles, as more PEG is being copolymerized. It should be noted that solubility parameters of MMA, nBA, and PFS are very similar, ranging from 8.8 to 8.2 cal/cm^3, which for PFS result from the highly polar C−F bonds and nonpolar benzene rings, thus making the overall solubility of PFS very similar to the other copolymerized monomers. As a result, random MMA/nBA/PFS copolymers are produced under monomer starvation conditions, and solid-state NMR data confirmed these results.

These data are in agreement with the NMR results and support the earlier assessments of the copolymer phase separation with the PEG phase being on the exterior. Initially, MMA, nBA, and PFS, being hydrophobic, migrate from monomer droplets to the polymerization site and copolymerize continuously under monomer starvation conditions to form p-MMA/nBA/PFS random copolymer. Since PEG exhibits significantly greater hydrophilicity and solubility in an aqueous medium, PEG molecules remain in the aqueous phase longer and react at the later stages of polymerization. This is depicted in Scheme 1A, steps 1 and 2. Although one could argue that PEG is physisorbed on the surface of MMA/nBA/PFS particles, NMR as well as zeta potential combined with solubility/reactivity data indicate its copolymerization forming phase-separating surface domains. As will be seen later, they will play a significant role in the film formation.

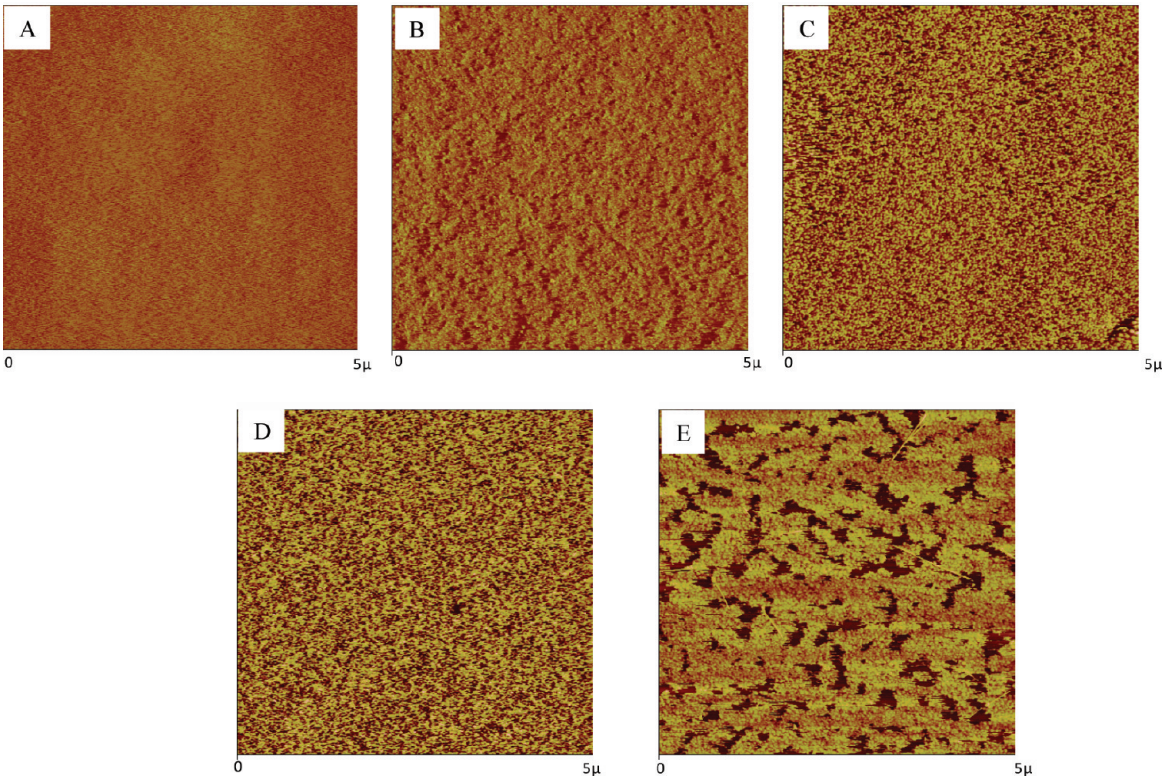

Figure 4. AFM phase images of (A) p-MMA/nBA/PFS, (B) p-MMA/nBA/PFS/PEG (5%), (C) p-MMA/nBA/PFS/PEG (10%), (D) p-MMA/nBA/PFS/PEG (20%), and (E) p-MMA/nBA/PFS/PEG (30%) copolymer films.

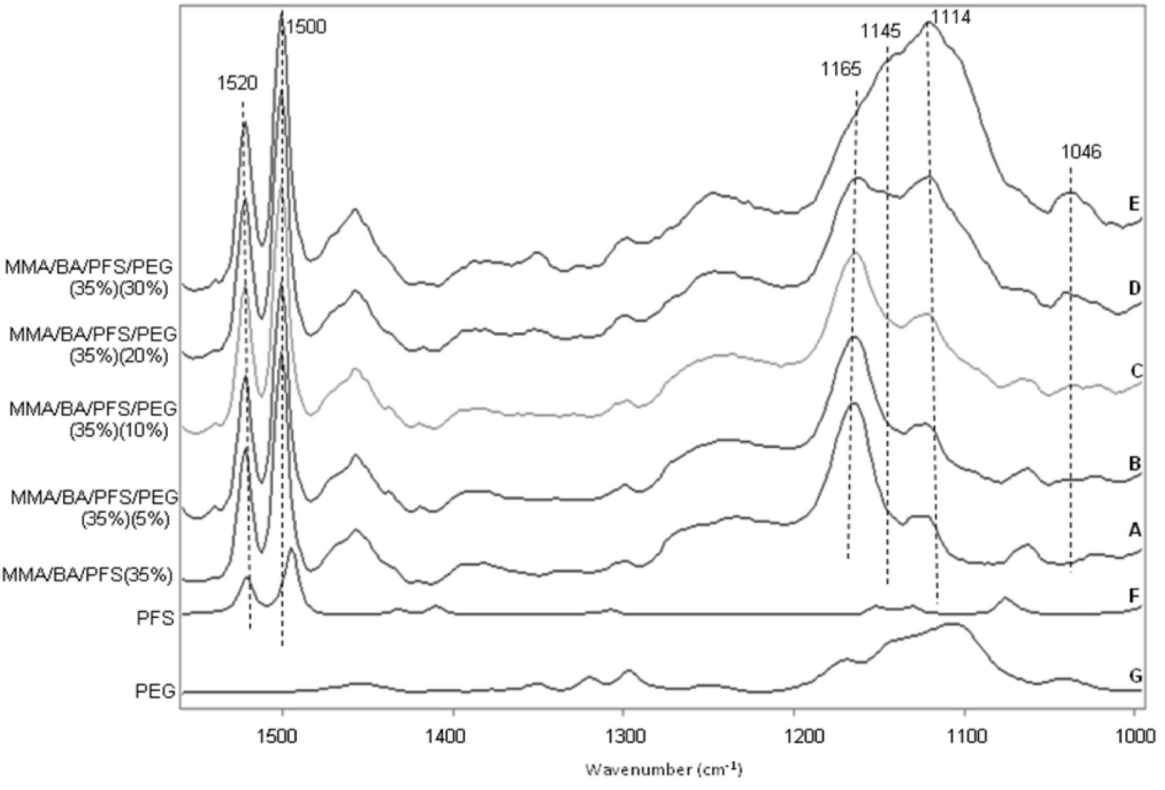

Figure 5. ATR FT-IR spectra of (A) p-MMA/nBA/PFS, (B) p-MMA/nBA/PFS/PEG (5%), (C) p-MMA/nBA/PFS/PEG (10%), (D) p-MMA/nBA/PFS/PEG (20%), (E) p-MMA/nBA/PFS/PEG (30%), (F) PFS monomer, and (G) PEG monomer.

p-MMA/BA/PFS/PEG Coalesced Films. The colloidal dispersions listed in Table 1 were allowed to coalesce, and their surface morphologies at the film−air (F−A) interface were analyzed using AFM. Figure 4A−E shows a series of AFM 5 × 5 μm phase images of the coalesced films of p-MMA/BA/PFS and p-MMA/BA/PFS/PEG containing 5, 10, 20, and 30% PEG (w/w), respectively. As shown in image A, a continuous one-phase component is observed and

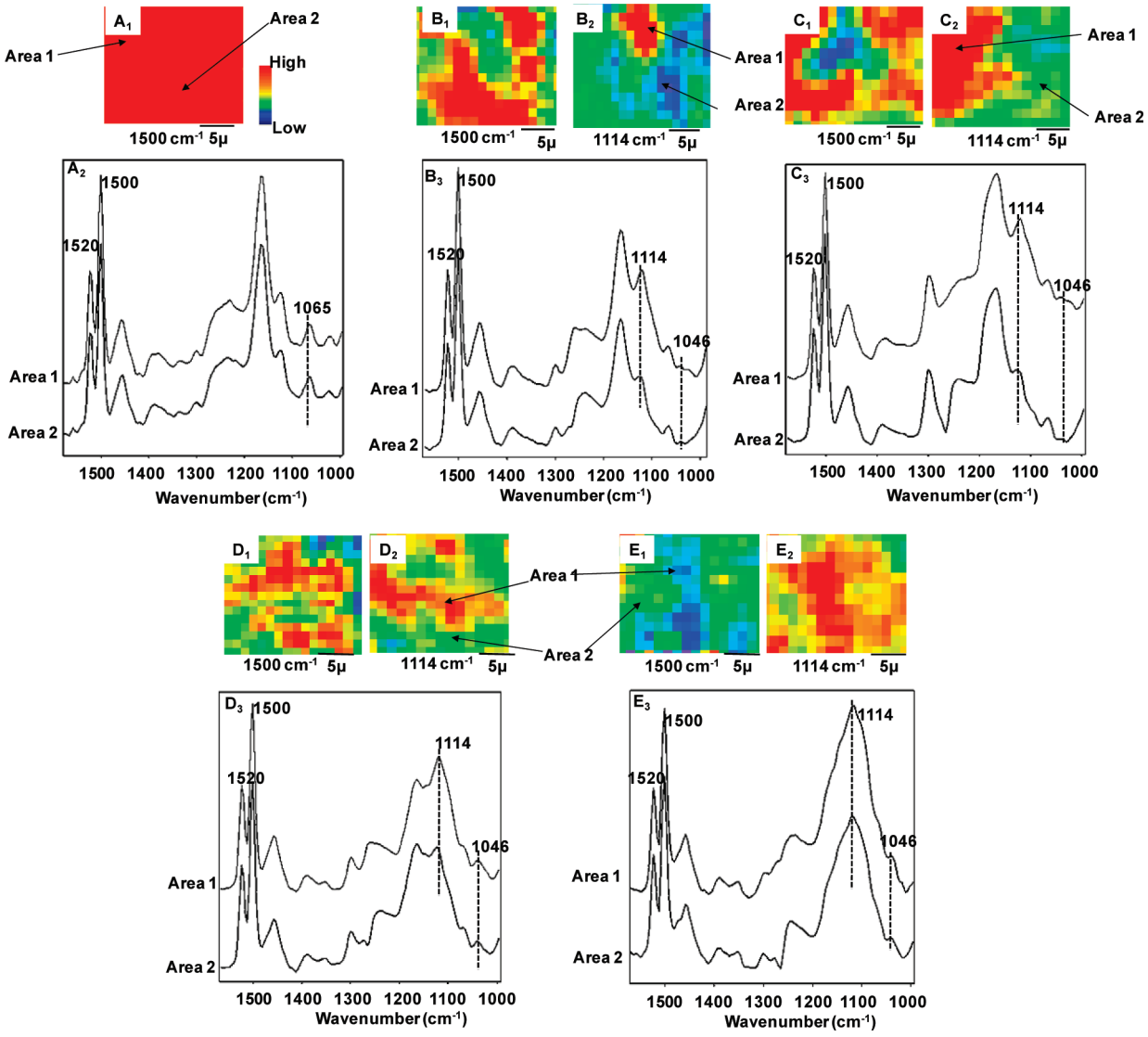

Figure 6. IRIR images recorded from the F−A interface of p-MMA/nBA/PFS (A_1), p-MMA/nBA/PFS/PEG (5%) (B_1), MMA/nBA/PFS/PEG (10%) (C_1), MMA/nBA/PFS/PEG (10%) (D_1), and MMA/nBA/PFS/PEG (10%) (E_1) colloidal films upon tuning to 114 and 1500 cm^{-1}; A_2, B_3, C_3, D_3, and E_3 represent IR spectra recorded from areas labeled 1 and 2 from corresponding images.

attributed to p-MMA/nBA/PFS at the F−A interface. However, upon introduction of PEG, phase separation is observed in images B−E, which is further enhanced upon higher (B) 5, (C) 10, (D) 20, and (E) 30% w/w content of PEG incorporated into p-MMA/nBA/PFS particles. The lighter areas of the images are attributed to the p-MMA/nBA/PFS (hard phase), whereas the darker regions are due to PEG regions (softer phase).

In order to verify chemical compositions at the F−A interface, ATR FT-IR spectra were recorded from the F−A interface. Figure 5A−E illustrates ATR FT-IR spectra recorded from the F−A interface of p-MMA/nBA/PFS (trace A), p-MMA/nBA/PFS/PEG (5%) (trace B), p-MMA/nBA/PFS/PEG (10%) (trace C), p-MMA/nBA/PFS/PEG (20%) (trace D), and p-MMA/nBA/PFS/PEG (30%) (trace E). For reference purposes, traces F and G illustrate the spectra of PFS and PEG. As expected, the band due to PEG at 1114 cm^{-1} increases as the PEG content increases. It should be pointed out that the same spectral features are observed at the F−S interface, thus showing that PEG distribution is uniform across the film thickness. The same applies to the PFS component of the film, as demonstrated by the unchanged intensities of the bands due to PFS at 1500 and 1520 cm^{-1} (C−F stretching). The 1165 and 1145 cm^{-1} bands due to C−O−C stretching vibrations of nBA and MMA components are also observed for all compositions. However, analysis of the spectra shown in Figure 5 also illustrates that SDOSS stratifies near to the F−A interface when PEG is incorporated, and the band at 1046 cm^{-1} due to $SO_3Na^+...H_2O$ associations increases upon the increasing PEG content (Figure 5, traces A−E) in colloidal dispersions.[35,37−40] The same behavior was confirmed in the previous studies.[41] Thus, during coalescence, as water evaporates, PEG retains H_2O molecules for the longest time, and SDOSS solubility in water facilitates environments for SDOSS to remain in the PEG phase.

As illustrated in Figure 4, AFM measurements (5 × 5 μm area) suggest stratification of phase-separated PEG component near the F−A interface. Since spatial resolution of IRIRI measurements is approximately 1 × 1 μm and these measurements provide molecular level information, combining AFM and IRIRI provides an opportunity for determining compositional heterogeneities shown in AFM images in Figure 4. Figure $6A_1$ represents the IR image obtained from p-MMA/BA/PFS films by tuning into the 1500 cm^{-1} band due to the C−F stretching vibrations of PFS. As seen, the

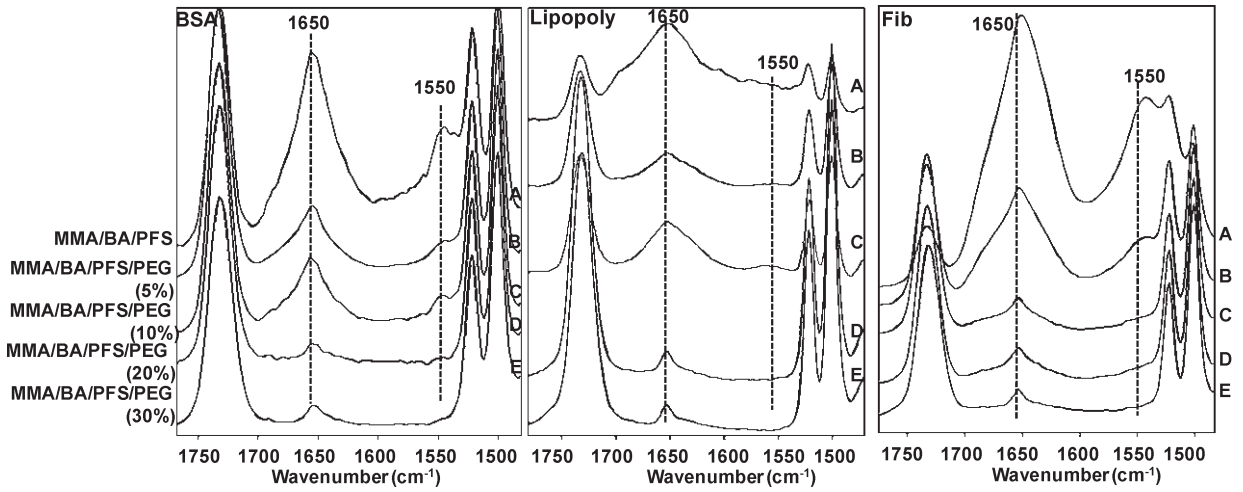

Figure 7. ATR FT-IR spectra recorded in the 1750−1500 cm^{-1} region of (A) p-MMA/nBA/PFS, (B) p-MMA/nBA/PFS/PEG (5%), (C) p-MMA/nBA/PFS/PEG (10%), (D) p-MMA/nBA/PFS/PEG (20%), and (E) p-MMA/nBA/PFS/PEG (30%) films exposed to BSA (a), Lipopoly (b), and Fib (c) proteins. The spectra were recorded after protein adsorption, followed by rinsing each specimen, as described in the Experimental Section.

Scheme 2. Schematic Representation of Protein Adsorption on (A) p-MMA/nBA/PFS and (B) p-MMA/nBA/PFS/PEG Films

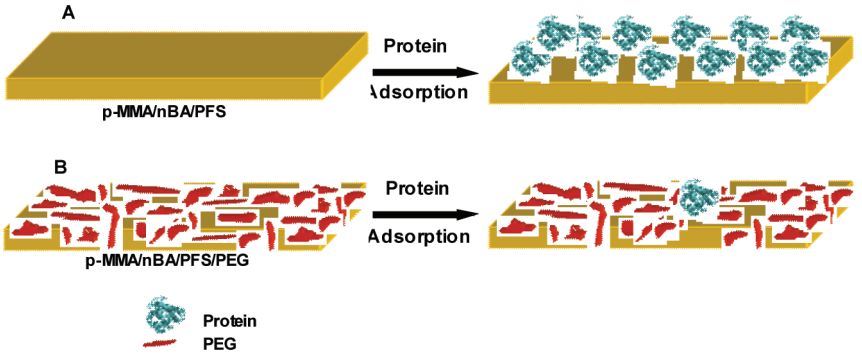

homogeneous distribution of PFS is observed for p-MMA/nBA/PFS films, which is also confirmed by IR spectra recorded from areas 1 and 2. As shown in Figure $6A_2$ there are no intensity differences between the 1500 and 1520 cm^{-1} bands. Thus, p-MMA/nBA/PFS colloidal particles exhibit uniform coalescence with no chemical compositional gradients near the interfacial regions. For the films containing p-MMA/nBA/PFS/PEG (5 wt %), IRIR images were obtained by tuning into the 1500 cm^{-1} band due to PFS as well as the 1114 cm^{-1} band due to C−O−C stretching vibrations of PEG. This is illustrated in parts B_1 and B_2 of Figure 6. As seen, the phase separation between the PFS and PEG is evident, as manifested by IR spectra recorded from areas 1 and 2 (Figure $6B_3$), where the spectrum recorded from area 1 exhibits higher intensities of the band at 1114 cm^{-1} due to PEG. The phase separation is further enhanced as the amount of PEG is increased to 10, 20, and 30 wt % (Figure 6, C_1 to C_3; Figure 6, D_1 to D_3; and Figure 6, E_1 to E_3). As seen, the domain size of the PEG phase is also significantly enhanced. As noted earlier in the ATR FT-IR analysis, the phase separation between p-MMA/nBA/PFS and PEG is also associated with the presence of the 1046 cm^{-1} band due to SDOSS...H_2O associations where the band increases as the amount of PEG incorporated in the colloidal dispersions is increased (Figure 6, A_1−E_3). Thus, the presence of PEG enhances the migration of SDOSS to the F−A interface, thus facilitating mobility of SDOSS molecules to the F−A interface during coalescence. On the basis of these data, the coalescence mechanism of p-MMA/nBA/PFS/PEG colloidal particles is schematically depicted in Scheme 1B. Because of the hydrophobic nature of p-MMA/nBA/PFS component containing phase separated hydrophilic PEG component, the two phases upon coalescence form phase-separated films with SDOSS molecules associated with water residing in the PEG phase as illustrated in Scheme 1B.

Protein Adsorption. Another objective of these studies was to examine protein adsorption properties of p-MMA/nBA/PFS/PEG films. To determine interactions between polymeric films containing p-MMA/nBA/PFS/PEG and proteins, we exposed the surfaces of the coalesced films to aqueous solutions containing BSA, Lipopoly, and Fib proteins for 2 h and analyzed their surfaces. To follow the protein adsorption process, ATR FT-IR spectroscopy was utilized. Figure 7 represents a series of ATR FT-IR spectra obtained from p-MMA/nBA/PFS/PEG films exposed to (a) BSA, (b) Lipopoly, and (c) Fib proteins, and traces B−E correspond to the increasing content of PEG. The amide 1 bands are detected at 1650 and 1550 cm^{-1} and manifest the presence of protein adsorption on the surface. As the PEG content increases, from 5 to 30% (traces B−E), the intensity of the amide band is reduced, thus inhibiting protein adsorption on the PEG surfaces.

Although it is anticipated that the presence of phase-separated PEG will alter protein adsorption, it is also of interest to identify if and how other components of the film participate in this process. To determine which phase is most susceptible for protein adsorption, IRIR images were collected from the films after exposure to BSA, Lipopoly, and Fib by tuning into the 1650 cm^{-1} bands due to −CO−NH linkages. The results of the IRIRI analysis are shown in

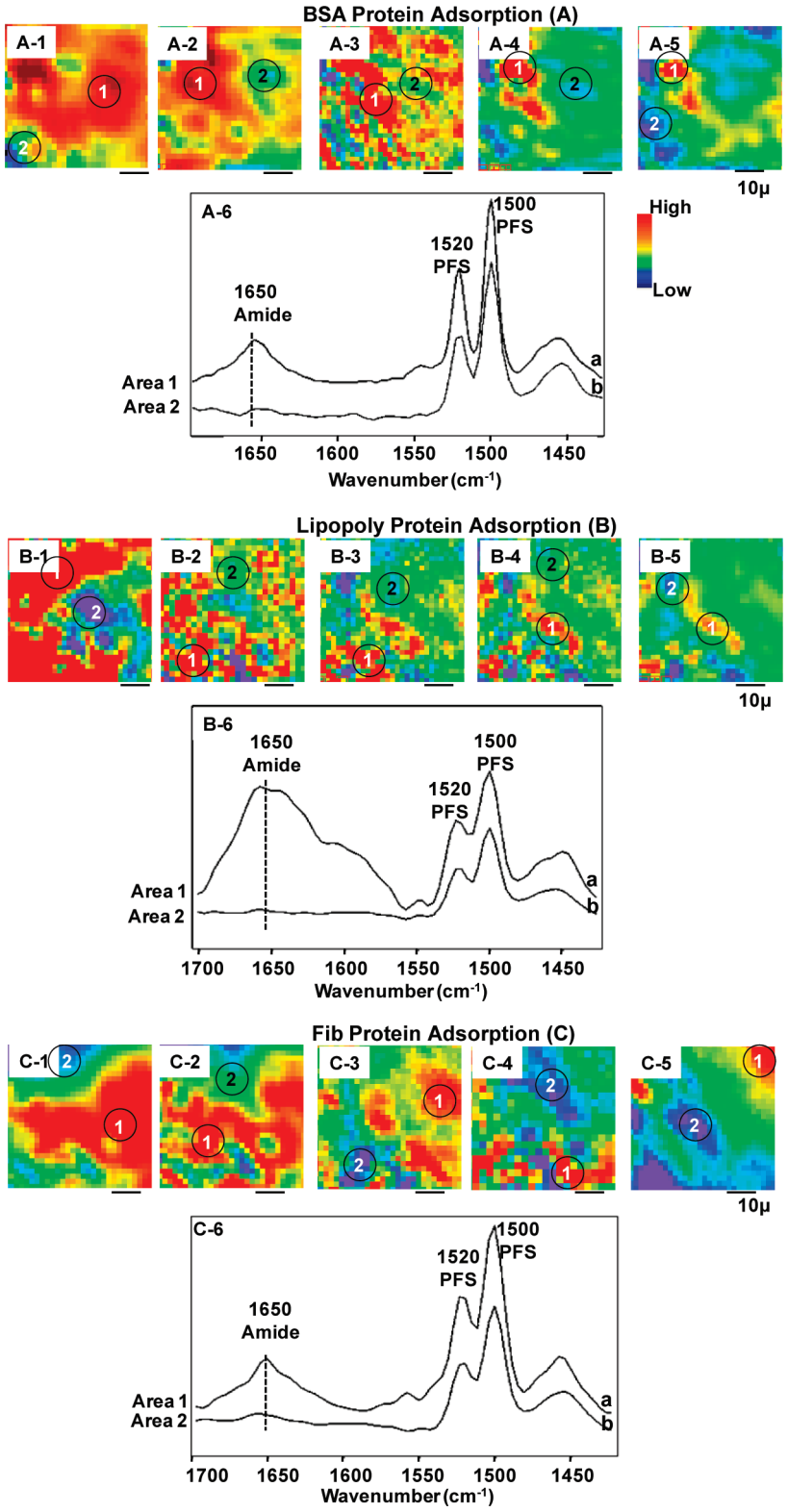

Figure 8. IRIR images recorded by tuning into the 1650 cm^{-1} band from the F−A interface of films exposed to BSA (A), Lipopoly (B), and Fib (C) proteins on (A-1, B-1, and C-1) p-MMA/nBA/PFS, (A-2, B-2, and B-2) p-MMA/nBA/PFS/PEG (5%), (A-3, B-3, and B-3) p-MMA/nBA/PFS/PEG (10%), (A-4, B-4, and B-4) p-MMA/nBA/PFS/PEG (20%), (A-5, B-5, and B-5) p-MMA/nBA/PFS/PEG (30%) copolymer films, and (A-6, B-6, and B-6) IR spectra recorded from areas labeled 1 and 2.

Figure 8A−C series by tuning into the 1650 cm^{-1} band due to amide I. As seen in Figure 8, A-1 through A-5 for specimens containing 0, 5, 10, 20 and 30% w/w PEG incorporated into p-MMA/nBA/PFS/PEG, the surface coverage with BSA is significantly reduced upon the increased PEG content. This is also supported by the analysis of the corresponding spectra recorded from the areas 1 and 2 of the A-4 image. The imaging results observed for Lipopoly (Figure 8B) and Fib (Figure 8C) proteins show similar results. Finally, the location of protein adsorption on the

copolymer surfaces is also of interest. Analysis of the amide I band at 1650 cm^{-1} shows that this band intensity increase parallels the enhanced intensity of the bands at 1500 and 1520 cm^{-1} due to PFS, thus suggesting that the preferential location of the protein adsorption is on the p-MMA/nBA/PFS phase. This is schematically depicted in Scheme 2A,B.

In summary, these studies showed a successful synthesis of stable p-MMA/nBA/PFS/PEG copolymer dispersions using free radical emulsion polymerization process. Up to 30% w/w of PEG can be copolymerized on to the exterior of p-MMA/nBA/PFS particles which upon coalescence form stable films capable of repelling proteins. Compositional heterogeneities between the PEG and PFS phases lead to a minimal affinity for proteins adsorption which predominantly occurs on the p-MMA/nBA/PFS surface domains.

Acknowledgment. Major support for these studies from the National Science Foundation Materials Research Science Engineering Center (NSF MRSEC) (DMR 0213883) is acknowledged.

References and Notes

(1) Gudipati, C. S.; Greenlief, C. M.; Johnson, J. A.; Prayongpan, P.; Wooley, K. L. *J. Polym. Sci., Part A: Polym. Chem.* **2004**, *42*, 6193–7.
(2) Bartels, J. W.; Cheng, C.; Powell, K. T.; Xu, J.; Wooley, K. L. *Macromol. Chem. Phys.* **2007**, *208*, 1676–82.
(3) Brady, R. F. *Biofouling* **2000**, *15*, 73–77.
(4) Chen, Y.; Liu, D.; Deng, Q.; He, X.; Wang, X. *J. Polym. Sci., Part A: Polym. Chem.* **2006**, *44*, 3434–9.
(5) Misra, A.; Jarrett, W. L.; Urban, M. W. *Macromolecules* **2007**, *40*, 6190–96.
(6) Yarbrough, J. C.; Rolland, J. P.; DeSimone, J. M.; Callow, M. E.; Finlay, J. A.; Callow, J. A. *Macromolecules* **2006**, *39*, 2521–7.
(7) Woodward, I.; Schofield, W. C.; Roucoules, V.; Badyal, J. P. S. *Langmuir* **2003**, *19*, 3432–8.
(8) Youngblood, J. P.; Andruzzi, L.; Ober, C. K.; Hexemer, A.; Kramer, E. J.; Callow, J. A.; Finlay, J. A.; Callow, M. E. *Biofouling* **2003**, *19* (Suppl.), 91–98.
(9) Vermette, P.; Meagher, L. *Colloids Surf., B* **2003**, *28*, 153.
(10) Morra, M. *J. Biomater. Sci., Polym. Ed.* **2000**, *11*, 547–51.
(11) Leckband, D.; Sheth, S.; Halperin, A. *J. Biomater. Sci., Polym. Ed.* **1999**, *10*, 1125–29.
(12) Kingshott, P.; Griesser, H. J. *Curr. Opin. Solid State Mater. Sci.* **1999**, *4*, 403–8.
(13) McPherson, T.; Kidane, A.; Szleifer, I.; Park, K. *Langmuir* **1998**, *14*, 176–180.
(14) Efremova, N. V.; Sheth, S. R.; Leckband, D. E. *Langmuir* **2001**, *17*, 7628–33.
(15) Malmsten, M.; Emoto, K.; Van Alstine, J. M. *J. Colloid Interface Sci.* **1998**, *202*, 507–602.
(16) Pasche, S.; De Paul, S. M.; Voros, J.; Spencer, N. D.; Textor, M. *Langmuir* **2003**, *19*, 9216–21.
(17) Otts, D. B.; Pereira, K. J.; Jarret, W. L.; Urban, M. W. *Polymer* **2005**, *46*, 4776–81.
(18) Otts, D. B.; Cueva-Parra, L. A.; Pandey, R. B.; Urban, M. W. *Langmuir* **2005**, *21*, 4034–40.
(19) Otts, D. B.; Urban, M. W. *Polymer* **2005**, *46*, 2699–2704.
(20) Powell, K. T.; Cheng, C.; Wooley, K. L.; Singh, A.; Urban, M. W. *J. Polym. Sci., Part A: Polym. Chem.* **2006**, *21*, 3044–50.
(21) Gudipati, C. S.; Finlay, J. A.; Callow, J. A.; Callow, M. E.; Wooley, K. L. *Langmuir* **2005**, *21* (7), 3044–3053.
(22) Gan, D.; Mueller, A.; Wooley, K. L. *J. Polym. Sci., Part A: Polym. Chem.* **2003**, *41* (22), 3531–3540.
(23) Finlay, J. A.; Krishnan, S.; Callow, M. E.; Callow, J. A.; Dong, R.; Asgill, N.; Wong, K.; Kramer, E. J.; Ober, C. K. *Langmuir* **2008**, *24*, 503–510.
(24) Yarbrough, J. C.; Rolland, J. P.; DeSimone, J. M.; Callow, M. E.; Finlay, J. A.; Callow, J. A. *Macromolecules* **2006**, *39* (7), 2521–2528.
(25) Sharma, S.; Johnson, R. W.; Desai, T. A. *Biosens. Bioelectron.* **2004**, *20*, 227–332.
(26) Popat, K. C.; Sharma, S.; Desai, T. A. *J. Phys. Chem. B* **2004**, *108*, 5185–5190.
(27) Sharma, S.; Johnson, R. W.; Desai, T. A. *Langmuir* **2004**, *20*, 348.
(28) Dreher, W. R.; Jarrett, W. L.; Urban, M. W. *Macromolecules* **2005**, *38*, 2205.
(29) Davis, S. D.; Hadgraft, J.; Palin, K. J. *Encyclopedia of Emulsion Technology*; Marcel Dekker: New York, 1985; Vol. *2*.
(30) Schaefer, J.; Stejskal, E. O.; Buchdahl, R. *Macromolecules* **1977**, *10*, 384.
(31) Schmidt-Rohr, K.; Clauss, J.; Spiess, H. W. *Macromolecules* **1992**, *25*, 3273.
(32) Tekely, P.; Palmas, P.; Mutzenhardt, P. *Macromolecules* **1993**, *26*, 7363.
(33) Urban, M. W. *Attenuated Total Reflectance Spectroscopy of Polymers - Theory and Practise*; 1989; Vol. *2*.
(34) Otts, D.; Zhang, P.; Urban, M. W. *Langmuir* **2002**, *18*, 6473.
(35) Evanson, K. W.; Thortenson, T. A.; Urban, M. W. *J. Appl. Polym. Sci.* **1991**, *42*, 2309.
(36) Brandrup, J.; Immergut, E. H. *Polymer Handbook*, 2nd ed.; John Wiley & Sons: New York, 1966.
(37) Zhao, Y.; Urban, M. W. *Macromolecules* **2000**, *33*, 7573.
(38) Niu, B. J.; Urban, M. W. *J. Appl. Polym. Sci.* **1996**, *62*, 1903.
(39) Thortenson, T. A.; Evanson, K. W.; Urban, M. W. *Polym. Mater. Sci. Eng.* **1991**, *64*, 195.
(40) Niu, B.-J.; Urban, M. W. *J. Appl. Polym. Sci.* **1996**, *60*, 371.
(41) Dreher, W. R.; Urban, M. W. *Langmuir* **2003**, *19*, 10254.